INTERNATIONAL JOURNAL OF HYDROGEN ENERGY 45 (2020) 1283–1296

Available online at www.sciencedirect.com

ScienceDirect

journal homepage: www.elsevier.com/locate/he

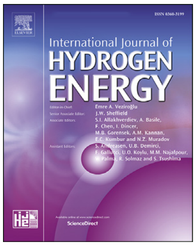

Combined experimental and theoretical study of acetylene semi-hydrogenation over Pd/Al_2O_3

Liliana P.L. Gonçalves [a,b], Jianguang Wang [c], Simone Vinati [d], Emanuele Barborini [d], Xian-Kui Wei [e], Marc Heggen [e], Miguel Franco [a], Juliana P.S. Sousa [a], Dmitri Y. Petrovykh [a], Olívia Salomé G.P. Soares [b], Kirill Kovnir [f,g], Jaakko Akola [c,h,**], Yury V. Kolen'ko [a,*]

[a] International Iberian Nanotechnology Laboratory (INL), Avenida Mestre José Veiga, 4715-330 Braga, Portugal
[b] Laboratory of Separation and Reaction Engineering — Laboratory of Catalysis and Materials (LSRE-LCM), Faculdade de Engenharia, Universidade do Porto, Rua Dr. Roberto Frias, 4200-465 Porto, Portugal
[c] Computational Physics Laboratory, Tampere University, P.O. Box 692, 33014 Tampere, Finland
[d] Tethis S.p.A., Milan 20143, Italy
[e] Ernst Ruska-Centre for Microscopy and Spectroscopy with Electrons and Peter Grünberg Institute, Forschungszentrum Jülich GmbH, 52425 Jülich, Germany
[f] Department of Chemistry, Iowa State University, Ames, IA 50011, United States
[g] Ames Laboratory, U.S. Department of Energy, Ames, IA 50011, United States
[h] Department of Physics, Norwegian University of Science and Technology, 7491, Trondheim, Norway

ARTICLE INFO

Article history:
Received 10 September 2018
Received in revised form
6 April 2019
Accepted 9 April 2019
Available online 9 May 2019

Keywords:
Heterogeneous catalysis
Hydrogenation
Kinetics
DFT
Modelling
Nanoclusters

ABSTRACT

The semi-hydrogenation of acetylene ($C_2H_2 + H_2 = C_2H_4$, $\Delta H = -172$ kJ mol^{-1}) is a well-studied reaction that is important for purification of ethylene, C_2H_4, feed used in polyethylene production. Pd-based catalysts are most commonly used to remove acetylene from ethylene feed prior to Ziegler–Natta polymerization because acetylene is a poison for Ziegler–Natta catalysts. New applications of the analogous catalytic processes, with similar requirements for the conversion and selectivity, are considered for the storage of H_2 within the context of the H_2 economy. Here, a combination of experimental and theoretical studies was employed to explore the performance of synthesized Pd nanoparticles and the feasibility of using computational modelling for predicting their catalytic properties. Specifically, a model 5%Pd/Al_2O_3 nanocatalyst was successfully synthesized using high-throughput flame spray pyrolysis (FSP) method. As a catalyst for acetylene semi-hydrogenation, the material shows high conversion of 97%, a modest selectivity of 62%, and a turnover frequency of ethylene formation of 5 s^{-1}. The experimental data were further supported by computational modelling of catalytic properties. Results of microkinetic simulations, based on parameters obtained from DFT calculations, over a $Pd_{30}/Al_2O_3(100)$ model system were correlated with experiments. The insights from this direct comparison of theory and experiments provide indications for future improvements of the theoretical predictions and for novel types of materials with improved catalytic properties.

---

* *Corresponding author.*
** *Corresponding author.* Department of Physics, Norwegian University of Science and Technology, 7491 Trondheim, Norway.
E-mail addresses: jaakko.akola@ntnu.no (J. Akola), yury.kolenko@inl.int (Y.V. Kolen'ko).
https://doi.org/10.1016/j.ijhydene.2019.04.086
0360-3199/

Introduction

An important industrial example of the semi-hydrogenation of acetylene, C_2H_2, to ethylene, C_2H_4 ($C_2H_2 + H_2 = C_2H_4$), is related to the need to reduce to a few ppm the acetylene concentration in the ethylene feedstock for polyethylene polymerization, which is typically produced from steam cracking of hydrocarbons and contains 0.5–2% of acetylene [1]. Without the catalytic semi-hydrogenation, this minor amount of acetylene negatively affects the polymerization process because acetylene poisons the Ziegler–Natta polymerization catalysts. Furthermore, to keep the process economically viable, the catalyst should not further convert ethylene into ethane, meaning that highly selective semi-hydrogenation of acetylene needs to be achieved [2,3]. Similar needs for improving the selectivity of catalysts [4] also emerge from the recent advances in the H_2 economy, whereby catalytic hydrogenation of unsaturated hydrocarbons, such as cyclohexane, methylcyclohexane, decalin, etc. [5] offers a promising pathway to store/use renewable H_2.

Pd-based catalysts have been employed in semi-hydrogenation of C_2H_2 to C_2H_4 due to their high activity for acetylene conversion. Unfortunately, these catalysts typically exhibit low selectivity because they subsequently convert C_2H_4 to unwanted C_2H_6 [6–8]. They also present limited stability caused by the accumulation of oligomers, which is mostly attributed to the fact that these catalysts provide active sites that enable side reactions [9–11]. An increase in the selectivity and stability of Pd catalysts has been achieved by, for example, the addition of promoters to the catalysts, or by mixing with other metals and metal oxides [12–17]. Despite the numerous studies addressing the improvement of Pd-based catalysts, it is still not possible to increase their selectivity and stability, a goal that requires understanding the catalytic reaction mechanism.

The reaction pathways of acetylene hydrogenation on Pd(111) surface have been investigated using first-principles DFT calculations, and the results revealed that the hydrogenation of acetylene to vinyl and vinyl to ethylene had similar activation barriers [18]. Later, using first-principles-based kinetic Monte Carlo simulations, Mei et al. reported that the simulated apparent activation energy, ethylene selectivity, and reaction orders were comparable with experiments [19]. More recently, semi-hydrogenation of acetylene over Pd-doped Cu(111) surfaces at low-temperature has been examined by DFT combined with microkinetic modelling [20]. It was found that the ethylene selectivity on a single-Pd-doped Cu(111) surface was higher than that of a monolayer-Pd-doped Cu(111), but the acetylene conversion exhibited inverse behaviors on these two surfaces. Until now, most theoretical studies have focused on the hydrogenation of acetylene over metal surfaces, while the investigations of Pd anchored on a supporting material remain a considerable challenge [21,22]. Accordingly, to develop advanced catalysts for semi-hydrogenation of C_2H_2, it is necessary to achieve a basic understanding of the catalytic reactions on model systems.

Herein, we report new synthesis, characterization, and catalytic hydrogenation properties of a Pd nanocatalyst supported on alumina, **Pd/Al_2O_3**. Moreover, we investigate whether state-of-the-art theoretical modelling can predict the catalytic behavior. The results of this study show a good agreement between the performed experiments and theoretical simulations, which opens a practical opportunity for computational screening of complex catalysts.

Experimental

Catalyst preparation

The flame spray pyrolysis (FSP) sample was produced employing a commercial FSP system (NPS10, Tethis, Italy). The NPS10 is a bench top system that allows the production of FSP nanopowder with laboratory mass-scale for R&D purposes. The burner where the pyrolysis reactions take place is described, for example, by Mädler et al. [23]. In our work, a liquid solution containing the metal organometallic precursors was injected, by a syringe pump (at a rate of 5 $cm^3\ min^{-1}$) through a stainless-steel capillary, into a nozzle where it was dispersed by an oxygen flow of 5 $dm^3\ min^{-1}$ (at a pressure drop of 1.5 bar). A concentric flamelet ring was fed with a premixed mixture of methane/oxygen (CH_4 1.5 $dm^3\ min^{-1}$, O_2 3.2 $dm^3\ min^{-1}$) for generating the supporting flame. Additional oxygen (5 $dm^3\ min^{-1}$) was supplied by an outer sheath flow to assure enough oxidant for complete conversion of the reactants. The powder was collected on a glassfiber filter (GF/A Whatman, Kent, United Kingdom), 150 mm in diameter. The filter was placed in a water-cooled holder 400 mm above the nozzle.

The liquid precursor was prepared by dissolving Pd(II)-acetylacetonate (99% Strem Chemicals) into acetonitrile (anhydrous, 99.8%, Sigma Aldrich) and then placing a suitable quantity of the obtained solution into a premixed solution of Al(III)-*sec*-butoxide (98%, Strem Chemicals) and xylene (Carlo Erba) in order to form a final solution of 0.69 M of Al. This synthesized sample will be referred to as **Pd/Al_2O_3 as-synthesized**. The obtained Pd loading was 5%, matching the loading of the reference commercial catalyst, which has been previously comprehensively characterized [11,24].

Catalyst Characterization

X-ray diffraction

Powder X-ray diffraction (XRD) patterns of the samples were obtained using a X'Pert PRO diffractometer (PANalytical) with a PIXcel 3D detector, set at 45 kV and 40 mA. The sample was ground to a fine powder and placed in the sample holder. A Bragg–Brentano configuration was used in a 2θ range from 20° to 80° with step size of 0.01° and a time per step of 300 s. Obtained data were analyzed with High Score software (PanAnalytical), matching the patterns to International Centre for Diffraction Data (ICDD) database.

Electron microscopy

A probe-corrected FEI Titan 80–200 Chemi-STEM microscope, equipped with a high-brightness Schottky field emission electron gun, was operated at 200 kV to carry out the structural and morphological analysis of the as-synthesized catalyst. The scanning transmission electron microscope (STEM) images were collected by a high-angle annular-dark-field (HAADF) detector in an angle range between 70 mrad and 200 mrad.

X-ray photoelectron spectroscopy

Supported catalyst powders were analysed in an ESCALAB 250 Xi system (Thermo Scientific). As-synthesized, oxidized, and reduced samples were scraped onto Al foil substrates and measured using a non-monochromatic Al Kα X-ray source (operating at 400 W power) to minimize charging artefacts. Peak fitting was performed in Avantage instrument software (Thermo Scientific), choosing a minimal number of components that produced random residuals consistently for all the samples. A convolution of Gaussian and Lorentzian line shapes was used for most of the spectral components; Pd 3d peaks required small asymmetric tails.

The binding energy (BE) scale is based on a BE shift (uniformly applied for all the samples) that placed the aliphatic C 1s peak associated with the supported catalyst material to 285.0 ± 0.2 eV, the value chosen based on previous measurements on non-metallic surfaces: polymer films [25], adventitious carbon [26], and alkane chains in self-assembled monolayers [27]. This BE correction places the (unresolved) Al 2p peak associated with the alumina of the catalyst support particles at 74.6 ± 0.2 eV.

Due to the apparent differential charging, there was a consistent (for all the samples) shift of 2.5 ± 0.1 eV between the high-resolution elemental peaks corresponding to the supported-catalyst particles and Al-foil substrate: aliphatic C 1s component as well as aluminum-oxide Al 2p and O 1s components. This differential charging shift enabled an unambiguous selection of the aliphatic C 1s component associated with the supported-catalyst particles to be used as the above-mentioned BE reference.

Nitrogen physisorption

The surface area, pore size, and pore volume of the samples were calculated with the determination of the N_2 adsorption–desorption isotherms of the samples at −77 K. The characterization was performed using a Quantachrome Autosorb IQ2 multi-station apparatus. Approximately 100 mg of sample was placed in the sample holder and outgassed under vacuum at 423 K for 240 min before the analysis. The specific surface area of the samples was determined according to the Brunauer–Emmett–Teller (BET) method in the range of ($0.05 < P/P_0 < 0.3$), the pore size was determined by the Barrett–Joyner–Halenda (BJH) method, and the pore volume was determined using the amount of vapor adsorbed at relative pressure close to unity ($P/P_0 = 0.97$).

Hydrogen chemisorption

H_2 chemisorption experiments on the Pd catalysts were performed on an AMI–200 Catalyst Characterization apparatus (Altamira) and using the pulsed method, in which pulses of 58 μL of H_2 are injected in the carrier gas (Ar, 25 $cm^3\ min^{-1}$) that flows through the sample, until the metal saturation, i.e., until the peak area becomes constant. The adsorbed hydrogen quantity is calculated by the integration of each peak that comes from each pulse, determined using a thermal conductivity detector (TCD). Before the analysis, the sample was preheated to 473 K in pure Ar flow and left for 1 h. Next, the flow was exchanged to a pure flow of hydrogen and the sample was reduced for 1 h. After the reduction, the system was purged with Ar and cooled down to 308 K. The hydrogen adsorption stoichiometry was assumed to be 0.5 H_2:Pd [28].

Catalytic measurements on acetylene semi-hydrogenation reaction

Catalytic measurements were performed in a continuous-flow fixed-bed quartz reactor with internal diameter of 7 mm, using quartz wool to trap the catalyst inside the reactor. The temperature in the bed was measured using a Type K thermocouple connected to a thermocouple data logger, and the gases, acetylene (2.6), hydrogen (5.0), and helium (5.0), were supplied using Bronkhorst mass flow controllers. The reaction products were analysed by a GC–2010 Plus from Shimadzu, equipped with a VP–Alumina column and a flame ionization detector (FID). The reactor was loaded with 1 mg of catalyst diluted in 100 mg silicon carbide (SiC) (60–80 mesh) and prior to each experiment, the catalyst was reduced *in situ* at 473 K for 30 min under a 20 $cm^3\ min^{-1}$ H_2 flow.

The conversion and selectivity of the catalysts were evaluated by isothermal and temperature-programmed experiments at atmospheric pressure for both the prepared sample after reduction (**Pd/Al_2O_3 reduced**) and commercial 5%Pd/Al_2O_3 catalyst (**Pd/Al_2O_3_Ref reduced**) (Alfa Aesar), which was used as reference. In the case of the isothermal experiments at 473 K, after the reduction treatment, the gas flow was changed to a mixture of 2% C_2H_2 and 20% H_2 balanced with helium at a total flow rate of 50 $cm^3\ min^{-1}$ and the time on stream was 9 h to evaluate the stability of the catalyst. For the temperature-programmed experiments, after reduction, the temperature was reduced to 300 K in 20 $cm^3\ min^{-1}$ helium flow and then the gas flow was changed to the same composition as in the isothermal experiments. The temperature was increased in 50 K steps at 10 K min^{-1}. In each step, the composition of the gas flow was analyzed after 30 min of stabilization.

The conversion on acetylene (X_{C2H2}) was calculated using the following equation:

$$X_{C2H2}(\%) = \frac{C_2H_2(feed) - C_2H_2}{C_2H_2(feed)} \tag{1}$$

Where C_2H_2(feed) is the concentration of acetylene on the feed and C_2H_2 is the concentration of acetylene in the product stream. The selectivity in ethylene formation (S_{C2H4}) was calculated as follows:

$$S_{C2H4}(\%) = \frac{C_2H_4}{C_2H_2(feed) - C_2H_2} \tag{2}$$

where C_2H_4 is the concentration of ethylene in the product stream.

The turnover frequency (TOF) was calculated as:

$$TOF = \frac{No.\ of\ C_2H_4\ molecules\ formed}{No.\ of\ exposed\ Pd\ sites\ on\ catalyst \times time} \tag{3}$$

The activation energy (E_a) for acetylene hydrogenation under the established conditions for the tested samples was calculated from the Arrhenius plot as:

$$E_a = -slope(Arrhenius\ plot) \times R \tag{4}$$

where R is the gas constant.

Computational modelling details

The structures and energies of the reactant, transition, and product states in acetylene hydrogenation over an alumina-supported Pd cluster were calculated using the density functional theory (DFT) methods as implemented in the CP2K program package [29,30]. All calculations were carried out spin-polarized within the generalized gradient approximation (GGA) using the Perdew, Burke, and Ernzerhof (PBE) exchange-correction potential [31] and analytical pseudopotentials of the type suggested by Goedecker, Teter, and Hutter (GTH) [32]. The Kohn–Sham wave functions were expanded in a double-zeta valence polarized (DZVP) basis set [33], which was optimized based on molecular properties. An auxiliary plane-wave basis with a 600 Ry kinetic energy cutoff was used to describe the electron density of valence electrons [34]. Only the Γ-point was employed for Brillouin zone integration as the model systems are laterally large and the alumina substrate (slab) is an insulator. The DFT-D3 method with the standard parameters suggested by Goerigk and Grimme was employed to correct the dispersion interaction [35]. Bader analysis of effective charges on atoms was used to determine the charge transfer [36,37], and the reaction paths were calculated using the climbing-image nudged elastic band (CI–NEB) method [38].

A periodic slab model was used for the support by cleaving a bulk γ-Al_2O_3 model [39] in the (100) direction. The Al_2O_3(100) support was chosen as a four-layer (4 × 3) slab (in total 480 atoms, lateral size 22.33×25.19 Å^2) and a vacuum spacing of at least 24 Å thickness in the vertical direction. The top two atomic layers were allowed to relax during the simulations while the bottom two layers were fixed. Here, a Pd_{30} cluster with the square-base pyramidal structure was chosen as a representative model catalyst structure. Previously, the same structure with 30 Pd atoms (*fcc*) was used for Pd and Pd–O clusters based on the correspondence with electron microscopy analysis [40]. To justify the Pd_{30}/Al_2O_3 model as a representative choice, a larger model catalyst composed of a pyramidal Pd_{55} cluster and an Al_2O_3(100) support with (5 x 3)-four-layer-slab (600 atoms, lateral size of 27.33×25.19 Å^2) has been tested. After optimization, Pd_{55} still displays the pyramid-like configuration with a base dimension of 10.71×10.78 Å^2. The nearest distances of cluster images are 16.6 and 14.4 Å in lateral directions, large enough to avoid interactions between cluster images, as imposed by periodic boundary conditions. The situation is comparable to the Pd_{30}/Al_2O_3 model where the corresponding image distances are 14.3 and 17.2 Å. For these two model structures, our DFT calculations reveal that the differences for acetylene adsorption energy (0.06 eV) and Bader charge on acetylene molecule (0.01*e*) are marginal. Meanwhile, the computational cost of the larger Pd_{55}/Al_2O_3 model is more than an order of magnitude more expensive. Thus, we consider the Pd_{30}/Al_2O_3 model structure both as feasible and representative for reaction modelling. Here, we need to declare that a larger model catalyst would need a much larger substrate to suppress cluster–cluster interactions due to periodic boundary conditions. This would lead to model structures of several thousands of atoms (most of them in the substrate), which is not feasible for DFT simulations in this context.

For acetylene hydrogenation over **Pd_{30}/Al_2O_3(100)**, it was assumed that atomic hydrogen is already available on the catalyst surface (See Supporting Information). Based on the co-adsorption configuration of $H^* + H^*$, the adsorption sites of C_2H_2 and C_2H_4 were optimized by considering different sites on the cluster surface. Here, the adsorption energy (E^2_{ads}) was calculated as

$$\begin{aligned} E^2_{ads} &= E(adsorbate) + E(Pd_{30}(H)_2/Al_2O_3) - E(adsorbate(H)_2 \\ &\quad + Pd_{30}/Al_2O_3 \end{aligned} \tag{5}$$

where E(Y) is the total energy of the corresponding system Y.

Microkinetic simulations were performed based on data (parameters) from DFT calculations over the **Pd_{30}/Al_2O_3(100)** model catalyst to study the acetylene hydrogenation under varying conditions [41–43]. The full details of the microkinetic model have been explained by Ma et al. [42]. The simulations were carried out at temperatures from 300 to 500 K, atmospheric pressure and feed composition of 2% C_2H_2 and 20% H_2. The kinetic values were estimated once the simulations were equilibrated to a steady state.

The acetylene conversion (X_{C2H2}) and ethylene formation selectivity (S_{C2H4}) were calculated as

$$X_{C2H2} = \frac{(R_{C2H4} + R_{C2H6})}{R_{C2H2}} \tag{6}$$

$$S_{C2H4} = \frac{R_{C2H4}}{(R_{C2H4} + R_{C2H6})} \tag{7}$$

where R refers to the reaction rate for the formation of the corresponding species.

Results

Characterization results

A 5% Pd on Al_2O_3 sample (**Pd/Al_2O_3 as-synthesized**) was prepared by flame spray pyrolysis (FSP), characterized, and tested for acetylene semi-hydrogenation reaction to achieve a basic understanding of the catalytic semi-hydrogenation of acetylene to ethylene on basic model systems. The powder XRD pattern of **Pd/Al_2O_3 as-synthesized** (Fig. 1) shows the characteristic peaks of cubic Al_2O_3 corresponding to the support, and the presence of PdO is confirmed by the presence of a peak at 2θ of ca. 34°.

By imaging using high-angle annular-dark-field technique in scanning transmission electron microscopy (HAADF–-STEM), PdO nanoparticles are observed to be uniformly anchored on the Al_2O_3 support (Fig. 2a). Statistical measurements reveal that sizes of the crystalline PdO particles on the

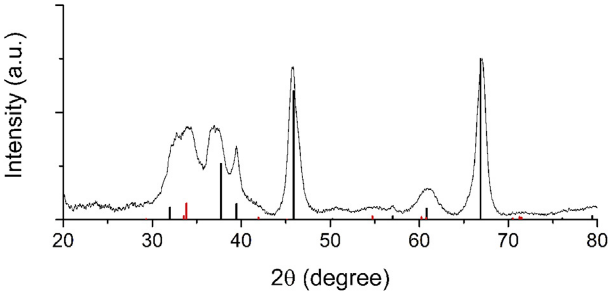

Fig. 1 – XRD pattern of the Pd/Al_2O_3 as-synthesized catalyst. Red lines: PdO; Black lines: Al_2O_3. (For interpretation of the references to color in this figure legend, the reader is referred to the Web version of this article).

Pd/Al_2O_3 as-synthesized sample are in the 1–5 nm range, and the Al_2O_3 supports have diameters in the 10–35 nm range. In Fig. 2b, close inspection of the morphology reveals that most of the PdO particles have elongated shapes and form agglomerates.

In addition to the XRD pattern, analysis by X-ray photoelectron spectroscopy (XPS) also reveals that the **Pd/Al_2O_3 as-synthesized** material contains Pd catalyst particles in their terminal PdO oxidation state. This conclusion is supported directly by the observed binding energy (BE) of the Pd $3d_{5/2}$ component at 336.9 eV (Fig. 3, top) [44]. The as-synthesized nature of this PdO oxidation state is indicated by the minimal changes in the XPS signatures of Pd 3d and C 1s produced by intentionally oxidizing the as-synthesized sample (Fig. 3, middle). In order to characterize the sample as it is used for the catalytic testing, XPS analysis was also performed after the reduction of the sample (**Pd/Al_2O_3 reduced**). In contrast to the as-synthesized sample, under reducing conditions the dominant Pd $3d_{5/2}$ component shifts to 335.3 eV (purple in Fig. 3, bottom), i.e., into the BE range of 335.1–335.4 eV previously reported [44,45] for metallic Pd. Furthermore, the chemistry of the associated organic material (solid symbols in C 1s region, Fig. 3) also undergoes an apparent reduction from oxidized to aliphatic (red and blue C 1s components in Fig. 3, respectively) [25].

To characterize the active surface area of the catalyst, H_2 chemisorption was performed on **Pd/Al_2O_3 reduced** and the results are summarized in Table 1. The average palladium particle size (d_M) determined by hydrogen titration is approximately 6 nm, while the particle size determined by HAADF–STEM is 2.85 nm. The palladium dispersion (D_M) is 19% and the metallic surface area (S_M) is 83 $m^2\ g^{-1}$. The BET specific surface area (S_{BET}), total pore volume (V_p), and pore width (d_p) of the **Pd/Al_2O_3 as-synthesized** catalyst were determined by N_2 physisorption, and the results are summarized in Table 1. The sample presents a surface area of 118 $m^2\ g_{cat}^{-1}$, a total pore volume of 0.3 $cm^3\ g_{cat}^{-1}$, and a pore width of 2 nm.

Catalytic measurements for acetylene semi-hydrogenation reaction

Fig. 4 presents the catalytic results, as a function of temperature and time on stream, of acetylene semi-hydrogenation reaction on **Pd/Al_2O_3 reduced** and **Pd/Al_2O_3_Ref reduced**, both reduced *in situ*; in this sub-section, these samples will be denoted as **Pd/Al_2O_3** and **Pd/Al_2O_3_Ref**, respectively. Fig. 4a presents the Arrhenius plot of ethylene formation TOF, from which the activation energy of acetylene hydrogenation is determined. Fig. 4b shows the variation of acetylene conversion (X_{C2H2}) and ethylene formation selectivity (S_{C2H4}) with temperature for both samples tested and Fig. 4c shows the same parameters as a function of time on stream.

Both samples display an increase in acetylene conversion and ethylene selectivity with temperature: in the case of the reference sample (**Pd/Al_2O_3_Ref**), X_{C2H2} increases from 23% at 325 K to 92% at 500 K and S_{C2H4} increases from 34% at 325 K to 56% at 500 K. For **Pd/Al_2O_3**, X_{C2H2} increases from 12% at 325 K to 97% at 500 K and S_{C2H4} increases from 42% at 325 K to 62% at 470 K. **Pd/Al_2O_3** behaves similarly to the reference sample, with somewhat higher selectivity for ethylene formation, for the tested temperatures. Regarding the stability, evaluated with the variation of X_{C2H2} and S_{C2H4} over time (Fig. 4c), both samples show similar X_{C2H2} values at 473 K over the tested time on stream, which decrease from 99% to 83% in the case of

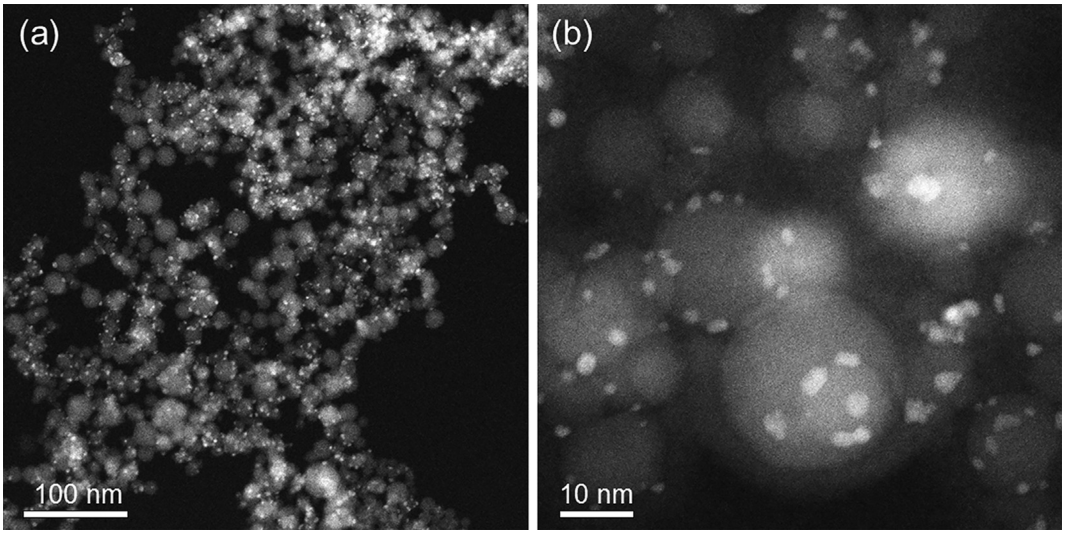

Fig. 2 – Low (a) and medium (b) magnification HAADF–STEM image of the Pd/Al_2O_3as-synthesized catalyst.

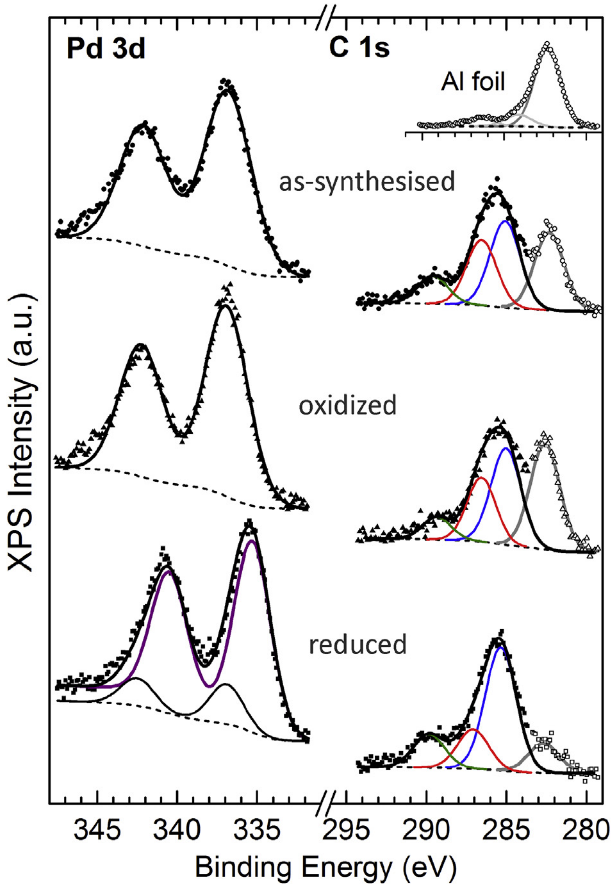

Fig. 3 – High-resolution XPS data for Pd 3d and C 1s regions. Supported catalyst powders were measured as-synthesized (Pd/Al_2O_3 as-synthesized) and after oxidation or reduction treatments (Pd/Al_2O_3 reduced) (top-to-bottom). Differential charging produced a consistent 2.5 eV shift between aliphatic C 1s components corresponding to the supported catalyst particles (blue lines, solid symbols) and Al-foil substrate (grey lines, open symbols, cf. top-right inset). Binding energy is presented after a correction (uniformly applied for all the catalyst samples), which placed the reference aliphatic C 1s peak (blue lines) at 285.0 ± 0.2 eV. Symbols: raw data; thick lines: overall fits; thin colored lines: fits of individual components; dashed lines: background. (For interpretation of the references to color in this figure legend, the reader is referred to the Web version of this article).

Pd/Al_2O_3 and from 97% to 85% for **Pd/Al_2O_3_Ref** after 9 h. In terms of S_{C2H4}, the value remains constant over 9 h of time on stream for both samples, with **Pd/Al_2O_3** showing a higher selectivity (≈70%) than **Pd/Al_2O_3_Ref** (≈60%).

The turnover frequency of ethylene formation was determined experimentally for the different temperatures tested and it increases with temperature, for both samples, reaching a value of 5 s^{-1} and 3 s^{-1} at 500 K for **Pd/Al_2O_3** and **Pd/Al_2O_3_Ref**, respectively. From the Arrhenius plot (Fig. 4a) it is possible to determine the activation energy (E_a) for acetylene hydrogenation under the established conditions for the tested samples. Sample **Pd/Al_2O_3** exhibits E_a of 5.0 ± 0.7 kcal mol^{-1}, while **Pd/Al_2O_3_Ref** exhibits E_a of 3.5 ± 0.6 kcal mol^{-1}.

DFT simulations and microkinetic modelling

Cluster–surface interaction

Fig. 5 gives the optimized model catalyst structure of **Pd_{30}/γ-$Al_2O_3(100)$**. Upon optimization, the Pd_{30} cluster still shows the pyramid-like structure with a base dimension of 8.03 × 7.95 $Å^2$ and average height of 5.78 Å. The optimized average Pd–Pd bond length is 2.76 Å, slightly larger than the 2.75 Å value in bulk Pd. The bond distances between the cluster base and support outermost layer vary in the range of 2.13–2.23 Å (Pd–O). The calculated cluster adsorption energy (E^{1}_{ads}) of Pd_{30} is 12.46 eV (0.195 eV $Å^{-2}$). Here, E^{1}_{ads} is defined as

$$E^{1}_{ads} = E(Pd_{30}) + E(Al_2O_3) - E(Pd_{30}/Al_2O_3) \qquad (8)$$

where *E(X)* is the total energy of the related system X. The Bader charge analysis reveals that the Pd_{30} cluster gains 1.64*e* of electron density in total, originating from the Al_2O_3 substrate, which makes the negatively charged catalyst prone to attract reactant molecules.

The projected density of states (PDOS) of electronic structure, charge density difference (CDD), and HOMO–LUMO orbital distributions are displayed in Fig. 6. PDOS (Fig. 6a) shows the projection of Kohn–Sham single-particle states onto atomic s-, p-, and d-components in the catalyst and support. At the Fermi energy, the weight of PDOS is significant on the cluster (Pd d-orbitals), while the support (insulator) exhibits a band-gap structure. In addition, the d-band center of Pd_{30} cluster, relative to the cluster Fermi energy, is calculated to be −2.00 eV, close to the experimental d-band centers in extended (bulk) Pd surfaces of −2.02 eV [46] and −2.09 eV [47]. The CDD visualization (Fig. 6b) displays a significant charge accumulation and depletion at the interface between the Pd_{30} cluster and Al_2O_3 substrate, providing more insight into the observed charge transfer. In particular, the accumulated charge is distributed around the cluster perimeter.

Table 1 – Textural properties of the Pd/Al_2O_3as-synthesized sample.

	Amount of surface-bound H_2[a] (μmol g_{cat}^{-1})	D_M[a] (%)	S_M[a] (m^2 g_{cat}^{-1})	d_M[a] (nm)	d_M[b] (nm)	S_{BET}[c] (m^2 g_{cat}^{-1})	V_p[c] (cm^3 g_{cat}^{-1})	d_p[c] (nm)
Al_2O_3	–	–	–	–	–	108	0.4	2
Pd/Al_2O_3	43.5	19	83	6.2	2.85	118	0.3	2

[a] Determined by H_2 chemisorption.
[b] Determined by HAADF–STEM.
[c] Determined by N_2 physisorption.

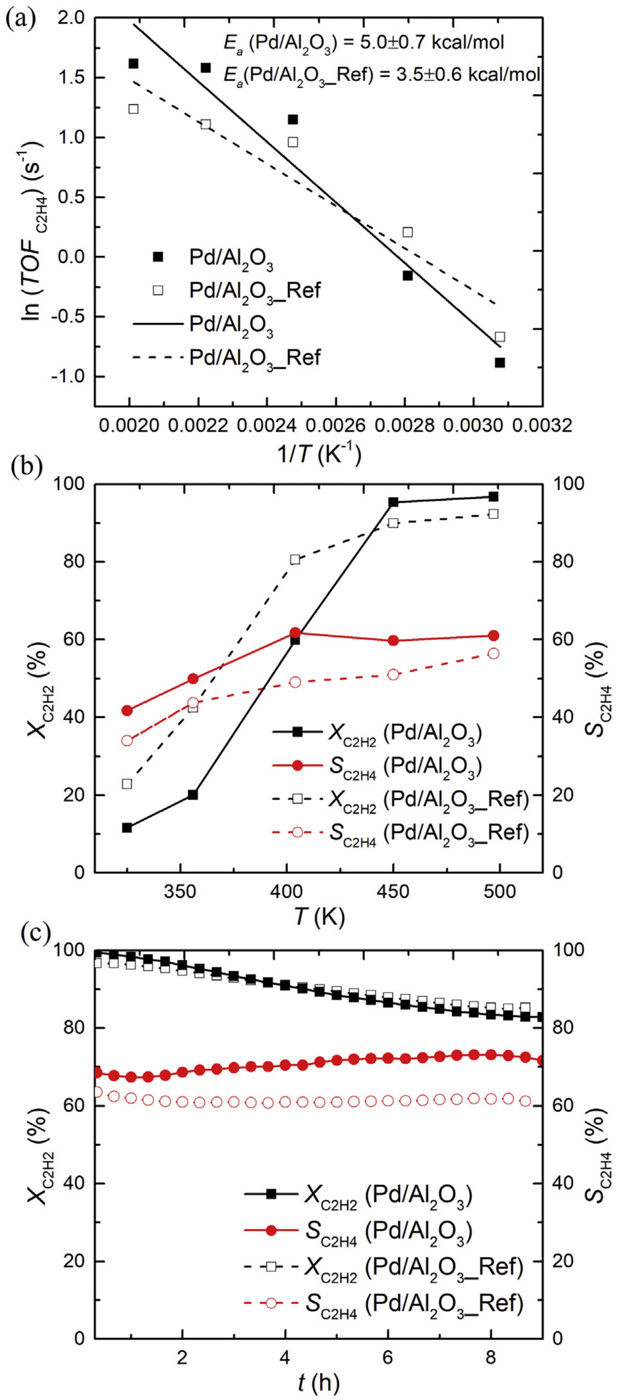

Fig. 4 – Catalytic measurement results as a function of the temperature and time on stream of acetylene semi-hydrogenation reaction on Pd/Al$_2$O$_3$ and Pd/Al$_2$O$_3$_Ref. The Arrhenius plot of ethylene formation TOF (a), acetylene conversion (X_{C2H2}), and ethylene formation selectivity (S_{C2H4}) as a function of the temperature (b) and time on stream (c).

Furthermore, the HOMO and LUMO orbital distributions (Fig. 6b) show that both states that are relevant to chemical reactivity are mainly delocalized within the Pd$_{30}$ cluster, with very small weight on the Al$_2$O$_3$ support.

Acetylene hydrogenation

The optimal adsorption site of the H$_2$ molecule was mapped by testing H$_2$ on different sites of the Pd$_{30}$ cluster surface, and the results are presented in supplementary material. Fig. 7 displays the structures of the initial state (IS), transition state (TS), intermediate state (IM), and final state (FS), and the energy diagrams along the hydrogenation pathways of acetylene to ethylene (Fig. 7a) and consecutive unwanted ethylene to ethane (Fig. 7b). At IS1, C$_2$H$_2$ binds on the hollow site of the Pd$_{30}$ surface with $E^2_{ads} = 2.11$ eV. The adsorbed C$_2$H$_2$ molecule receives 0.16e electron density from the catalyst. During the acetylene hydrogenation reaction, C$_2$H$_2$ is first hydrogenated to C$_2$H$_4$ by attaching two H atoms through TS1, IM1, and TS2 along the reaction pathway as shown in Fig. 7a. In the first transition state (TS1), H atom moves to the adjacent Pd top site from its original hollow site with a H–Pd and H–C bond of 1.57 and 1.65 Å, respectively. At the same time, the orientation of C$_2$H$_2$ also changes slightly, and the activation barrier is 0.72 eV (TS1). After this, the first intermediate state (IM1) of C$_2$H$_3$ is formed with an exothermic energy of 0.05 eV. The activation barrier for the second H atom (TS2) is 0.75 eV with H–Pd and H–C bond lengths of 1.57 and 1.88 Å, respectively. The first product molecule of C$_2$H$_4$ is formed in FS1 by the H atom binding to C$_2$H$_3$ and the reaction energy is −0.36 eV.

Following the first-step hydrogenation of C$_2$H$_2$ to C$_2$H$_4$, two additional H atoms were placed on the same hollow sites of the Pd$_{30}$ surface. C$_2$H$_4$ prefers to bind on a bridge site of the Pd$_{30}$(H)$_2$ surface with the adsorption energy of 1.33 eV and a net charge of −0.05e. Next, C$_2$H$_4$ is hydrogenated to the final product (FS2) of C$_2$H$_6$ by attaching H atoms one-by-one. The reaction pathway in Fig. 7b includes two transition states with activation barriers of 0.92 eV (TS3) and 0.81 eV (TS4) and one intermediate (IM2, C$_2$H$_5$) with reaction energy of 0.26 eV. The corresponding higher activation barriers give the first indication for ethylene selectivity. The final product of C$_2$H$_6$ (FS2) is generated with an exothermic energy of −0.10 eV. The C–C and C–H bond lengths of the C$_2$H$_6$ molecule are 1.53 and 1.10 Å (1.54 and 1.11 Å in gas phase), respectively.

Microkinetic simulations

Fig. 8 displays the microkinetic results for the temperature dependence of the Arrhenius plot of ethylene formation TOF, acetylene conversion (X_{C2H2}), and ethylene formation selectivity (S_{C2H4}), and the surface coverages of hydrogen (θ_H) and acetylene (θ_{C2H2}). The simulations show that the TOFs of ethylene increase with temperature. The apparent activation energy (E_a) of acetylene hydrogenation is 8.8 ± 0.6 kcal mol^{-1} by fitting the Arrhenius plot in Fig. 8a. Here, we need to emphasize that this apparent activation energy is different from the DFT-calculated activation barriers in the elementary reaction steps, as shown in Fig. 7.

The simulated results of X_{C2H2} and S_{C2H4} as a function of temperature are plotted in Fig. 8b. Both increase with the temperature between 300 and 500 K; X_{C2H2} increases from 80%

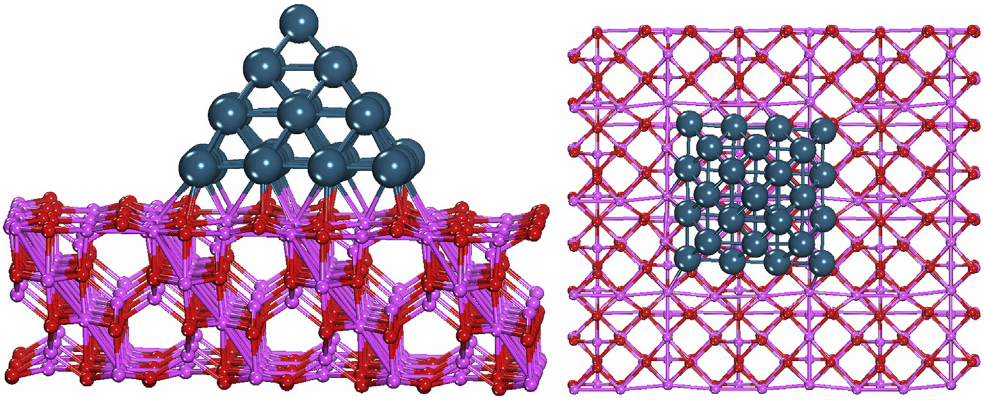

Fig. 5 – **Model structure (side view and top view) of a pyramidal Pd_{30} cluster on γ-Al_2O_3 (100) surface. Color key: Pd, dark green; O, red; Al, pink. (For interpretation of the references to color in this figure legend, the reader is referred to the Web version of this article).**

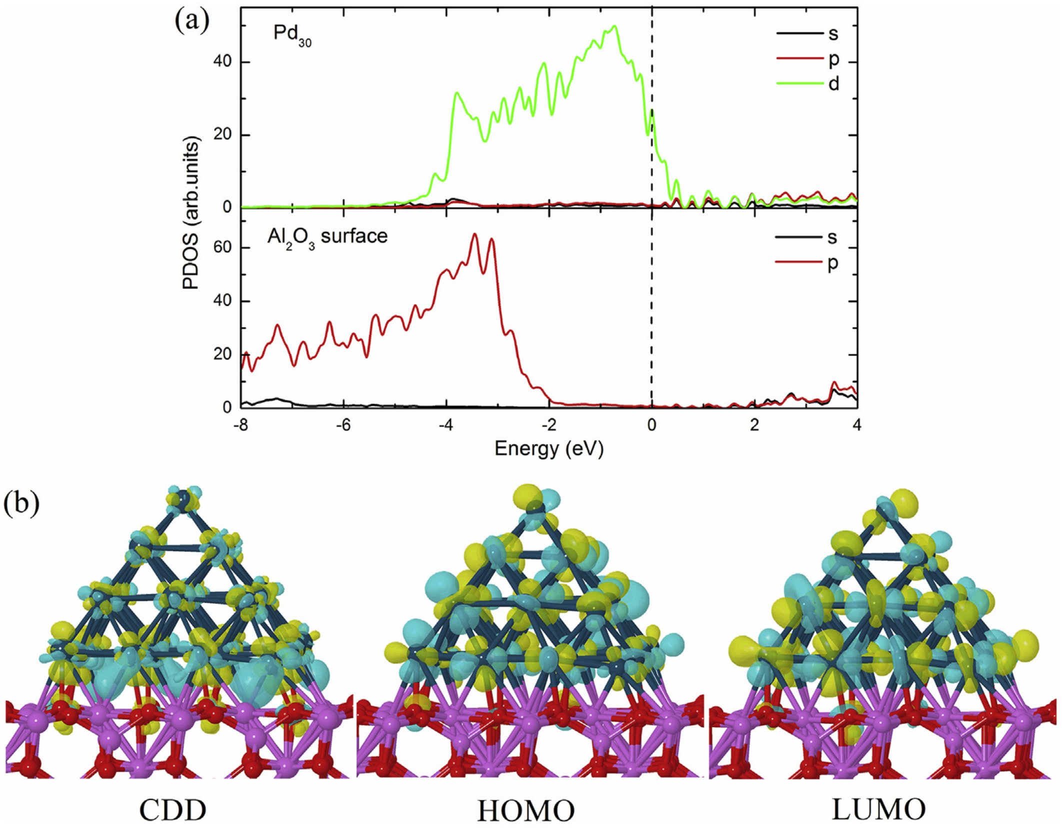

Fig. 6 – **The electronic properties of $Pd_{30}/Al_2O_3(100)$ system: (a) Projected density states (PDOS) on the atomic s-, p-, and d-orbitals in the cluster and support, respectively. The vertical line indicates the Fermi level. (b) Side view of charge density difference (CDD) and HOMO–LUMO orbitals. The yellow and aqua colors for CDD represent charge depletion and accumulation, respectively. For HOMO/LUMO these colors represent the different signs of the wavefunction. The isosurface values are ±0.002 e a_0^{-3} for CDD and ±0.01 e a_0^{-3} for HOMO and LUMO. (For interpretation of the references to color in this figure legend, the reader is referred to the Web version of this article).**

at 300 K to 100% at 400 K, and S_{C2H4} increases from 90% at 300 K to 99% at 470 K. The formation of C_4 and C_6 byproducts are not included in the current simulations, which can lower the ethylene selectivity at the lower temperature [48].

The surface coverages of all species were also examined, and those for hydrogen (θ_H) and acetylene (θ_{C2H2}) are plotted as a function of temperature in Fig. 8c. They exhibit opposite behavior with increasing temperature: θ_H decreases from 0.11 ML at 300 K to 0.06 ML at 450 K, while θ_{C2H2} increases from 0.58 ML at 300 K to 0.70 ML at 500 K. Furthermore, the surface coverages of vinyl, ethylene, and ethyl (not shown) are very low in the range of the temperatures considered herein.

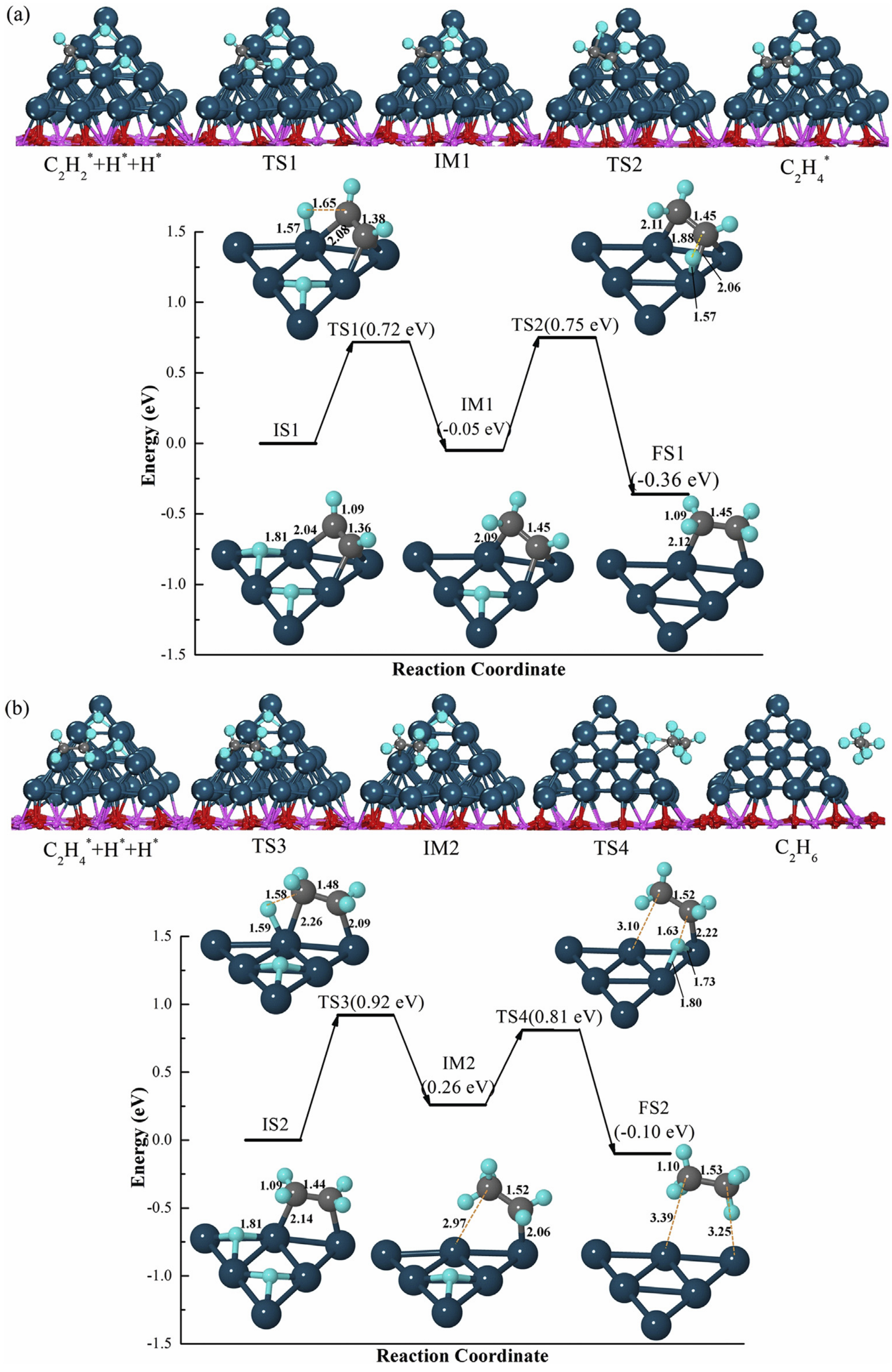

Fig. 7 – Structures of the initial state (IS), transition state (TS), intermediate state (IM), and final state (FS), and the energy diagrams along the hydrogenation pathways of (a) acetylene to ethylene ($C_2H_2^* + H^* + H^* \rightarrow C_2H_4^*$), and (b) ethylene to ethane ($C_2H_4{}^* + H^* + H^* \rightarrow C_2H_6$) over $Pd_{30}/Al_2O_3(100)$. The energy diagrams display the reactants/products and a cluster (111)-facet (only fraction of the cluster). The geometrical parameters (in Å) are also given. The symbol * refers to the atom or molecule being adsorbed on the catalyst. Color key: Pd, dark green; H, aqua; C, gray; O, red; Al, pink. (For interpretation of the references to color in this figure legend, the reader is referred to the Web version of this article).

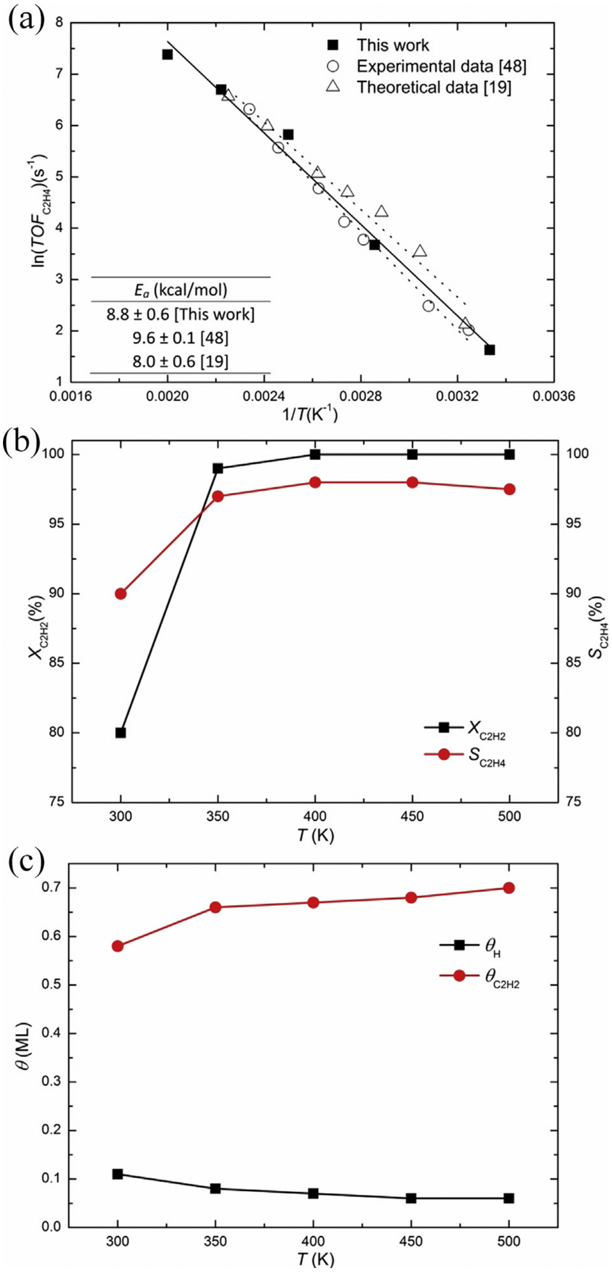

Fig. 8 – Microkinetic modelling results as a function of temperature in acetylene hydrogenation over Pd_{30}/Al_2O_3(100). (a) Arrhenius plot of ethylene formation TOF, (b) acetylene conversion (X_{C2H2}) and ethylene formation selectivity (S_{C2H4}), and (c) surface coverage of hydrogen (θ_H) and acetylene (θ_{C2H2}).

Discussion

Here, we present a combined approach using both experimental and theoretical studies to develop and validate a theoretical model for predicting the behavior of catalysts. Typically, it is possible to find overlapping experimental and theoretical studies in the literature, however, combined approaches are rather rare. A Pd/Al_2O_3 catalyst (**Pd/Al_2O_3 as-synthesized**) was synthesized using the flame spray pyrolysis method, a typical method for catalyst preparation, and it was used as standard catalyst, after *in situ* reduction (**Pd/Al_2O_3 reduced**), to test the theoretical model obtained through computational simulations. The performance of a representative Pd_{30} cluster was simulated and it was compared with the real Pd catalyst on alumina to confirm the success of the developed model.

The characterization of the **Pd/Al_2O_3 as-synthesized** sample by XRD showed that the Pd catalyst nanoparticles are in the PdO state (Fig. 1), which is expected due to oxidation of the catalysts during synthesis because of high oxidation conditions present in the flame. This result was confirmed by XPS analysis with the binding energy of the Pd $3d_{5/2}$ (Fig. 3), which is in excellent agreement with the BE of 336.8 eV previously reported by Brun et al. [44] for a reference PdO powder. However, as shown by the XPS results, after reduction (**Pd/Al_2O_3 reduced**), the dominant Pd $3d_{5/2}$ component is in the range of 335.1–335.4 eV, previously reported [44,45] for metallic Pd, which means that the catalyst nanoparticles are metallic Pd after *in situ* reduction and before reaction. XPS confirms the reduction of the associated organic material from oxidized to aliphatic, thus, supporting the conclusion that both Pd and organic constituents of the sample become oxidized during synthesis rather than due to subsequent exposure to air. We note that the 0.5–3 eV higher BE values reported for the metallic and oxidized Pd supported on insulating (e.g., alumina [49] or zeolite [50]) particles may result from the ambiguous nature of the C 1s component assigned as the aliphatic-carbon BE reference: The possible artifacts due to differential charging are highlighted by the 2.5 eV separation explicitly observed in this work between the spectral signatures derived from the Al-foil substrate and the supported catalyst particles (open and solid symbols in Fig. 3, respectively).

The HAADF–STEM shows, as expected, that the catalyst prepared using flame spray pyrolysis (**Pd/Al_2O_3 as-synthesized**) yielded spherical PdO particles with an average size of 2.85 nm (Table 1), uniformly distributed on the supporting material (Fig. 2). The obtained average size and particle shape is similar to those reported, for example, by Strobel et al. [51] for Pd on alumina also prepared by FSP, which presents spherically shaped Pd nanoparticles with an average size of 2.7 nm. The structure and morphology of the support were maintained after the deposition of the Pd nanoparticles (Table 1). The specific surface area (S_{BET}), pore volume (V_p), and pore diameter (d_p) are similar for the used Al_2O_3 support and for the **Pd/Al_2O_3 as-synthesized** catalyst, which confirms that the deposition of the Pd nanoparticles did not alter the microstructure of the support. Similarly to the Pd particle size, the microstructure of our sample is comparable to the properties of the catalyst prepared by Strobel et al. [51], which had a specific surface area of 120 m^2 g_{cat}^{-1}.

The particle size was determined both by HAADF–STEM on the **Pd/Al_2O_3 as-synthesized** sample and H_2 chemisorption on the **Pd/Al_2O_3 reduced** catalyst (Table 1), and the particle size obtained from H_2 chemisorption is higher. This discrepancy is due to the different weighting of the two procedures: chemisorption determines the surface-area weighted diameter, while HAADF–STEM determines the number-average diameter. Importantly, the value determined by chemisorption provides valuable information for heterogeneous catalysis, as it is related to the active metallic surface area. The values of Pd

Table 2 – Comparison of catalyst performance determined experimentally (Exp) and theoretically (Theo).

Catalyst	X_{C2H2} (%) at 450 K	S_{C2H4} (%) at 450 K	E_a (kcal mol^{-1})	m_{cat} (mg)	Feed composition (C_2H_2:H_2)		Ref.
Pd/Al_2O_3	80	75	–	0.5	1:2	Exp	[12]
Pd foil	–	94[a]	9.6 ± 0.1	–	1:1	Exp	[48]
Pd (111)	–	95	8.0 ± 0.6	–	1:1	Theo	[19]
Pd/Al_2O_3	95	60	5.0 ± 0.7	1	1:10	Exp	This work
Pd/Al_2O_3_Ref	90	51	3.5 ± 0.6	1	1:10	Exp	This work
Pd_{30}/Al_2O_3	100	98	8.8 ± 0.6	–	1:10	Theo	This work

[a] Determined for conversions <1%.

dispersion and particle size obtained by H_2 chemisorption (Table 1) are comparable to those obtained by Strobel et al. [51] using CO chemisorption.

The results obtained for the conversion and selectivity of the **Pd/Al_2O_3 reduced** and **Pd/Al_2O_3_Ref reduced** samples (Fig. 4) are similar, which confirms that **Pd/Al_2O_3 reduced** can be used as a model catalyst since it behaves similarly to the commercial reference sample. In addition, the obtained results agree with those found in the literature [12,48] in the range of the tested temperatures. In this work, to simplify the theoretical simulations, a simplified gas mixture was used, neglecting the large excess of ethylene common in the industrially relevant feed composition (non-competitive conditions). Thus, the results were compared to studies where the excess of ethylene was also omitted. Table 2 presents a comparison of the experimental results obtained in this work with those reported in the literature for similar catalysts.

Osswald et al. [12] tested Pd on Al_2O_3 reference catalyst, which achieved a maximum conversion at 450 K, and a similar temperature dependence of activity was observed in the current work (Fig. 4). The activity reported by Osswald et al. at 450 K is lower (≈80%) than that obtained for both samples here (95% and 90%). The catalysts studied by Osswald et al. exhibit higher selectivity in the 350–500 K interval, ranging from 60% to 80% [12]. Molero et al. [48] tested a palladium foil sample for acetylene semi-hydrogenation, where the selectivity increased drastically from approximately 30% at 300 K to 94% at 470 K. Considering the selectivity and conversion results, the sample prepared and tested in this study exhibits a similar overall trend compared to the results found in the literature, however, with slightly different selectivity [12,48]. We note that these differences in the selectivity and conversion values can be due to differences in the experimental conditions, i.e., different feed composition and mass of catalyst used. Osswald et al. [12] used a feed composition of 2% acetylene and 4% hydrogen in helium and 0.5 mg of catalyst, while Molero et al. [48] performed the reaction with a ratio of acetylene to hydrogen of 1:1.

In terms of stability, the selectivity values in Fig. 4c agree with previous studies [12], but the conversion rate has a smaller decrease compared to the study of Osswald et al. [12], where the stability of a reference Pd on alumina catalyst was also tested and the conversion decreased from 100% to around 20% after 9 h, while the selectivity was approximately stable at 60% [12]. As above, we note that the reaction conditions used in Ref. [12] are different from ours.

Our computational studies suggest a comparable catalytic activity for acetylene hydrogenation on a Pd_{30} cluster and on Pd surfaces, as expected based on the similar d-band centers of these systems (Fig. 6a). However, the microkinetic simulations (Fig. 8) predict a higher activity and selectivity for the Pd_{30} clusters, and the predicted trends agree with those obtained in the experimental results (Fig. 4). The selectivity for ethylene determined in the microkinetic simulations agrees well with the previous results for simulations [19] and experiments for surfaces [48] in the same range of temperatures.

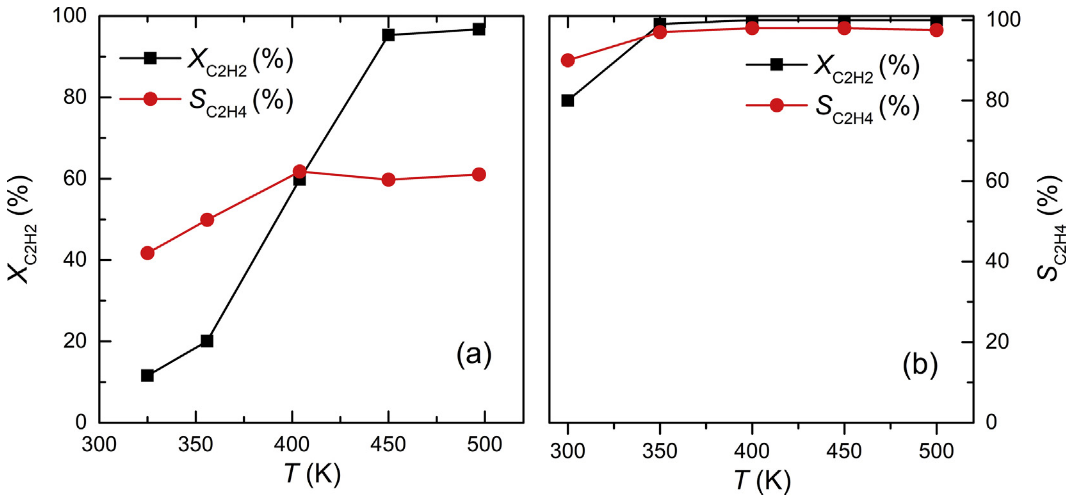

Fig. 9 – Acetylene conversion (X_{C2H2}) and ethylene formation selectivity (S_{C2H4}) as a function of temperature determined experimentally (a) and theoretically (b).

The quantitative differences between the experiments (**Pd/Al_2O_3 reduced**) and theory (**$Pd_{30}/Al_2O_3(100)$**) can be explained by the particle size: the clusters in **$Pd_{30}/Al_2O_3(100)$** are considerably smaller than the Pd nanoparticles on **Pd/Al_2O_3 reduced**, which explains the lower experimental selectivity. The larger Pd nanoparticles favor the formation of the β-hydride phase, which supplies active hydride species to surfaces resulting in full hydrogenation of acetylene to ethane, thus decreasing the ethylene selectivity [52,53]. Furthermore, our microkinetic model has been parameterized at low coverage limit which may affect the results.

The computed activation energy over **$Pd_{30}/Al_2O_3(100)$** (8.8 ± 0.6 kcal mol^{-1}) is comparable to the experimental value obtained by Molero et al. [48] of 9.6 ± 0.1 kcal mol^{-1} over a clean Pd foil, and with the computed one by Mei et al. [19] of 8.0 ± 0.6 kcal mol^{-1} over Pd(111), at the conditions of $P(H_2) = P(C_2H_2) = 100$ Torr and temperature range of 300–500 K, but the activation energy obtained experimentally for the **Pd/Al_2O_3 reduced** sample is slightly lower (5.0 ± 0.7 kcal mol^{-1}). Again, these values are sensitive to the experimental conditions (feed composition), catalyst itself (film, nanoparticle), as well as synthetic history.

Fig. 9 shows the comparison between the acetylene conversion (X_{C2H2}) and ethylene formation selectivity (S_{C2H4}) results as a function of temperature determined experimentally and theoretically. It can be observed that the results obtained experimentally with the **Pd/Al_2O_3 reduced** catalyst qualitatively agree with the microkinetic simulations based on parameters from extensive DFT calculations over a **$Pd_{30}/Al_2O_3(100)$** model catalyst. The predicted and experimental conversions agree well at temperatures above 450 K, while selectivities and conversions at lower temperatures are different, apart from the agreement in the general trend of increasing of activity and selectivity with temperature. In addition to the aforementioned reasons, the mismatch between theory and experiment may be due to simplifications used in the modelling, where the dissolution of hydrogen and carbon in the Pd subsurface region were not considered [52]. More expensive calculations where the structure of the Pd cluster is flexible and can be refined are required to improve the theoretical results. Nevertheless, the good agreement at high temperatures shows that the model used in this study can be used for fast screening of potential catalysts, especially of intermetallic catalysts with covalent bonding, where the dissolution of hydrogen or carbon is suppressed [24]. Conversely, the high selectivity predicted by the theory indicates that novel material designs that attempt to minimize the dissolution of hydrogen and carbon in Pd should be considered for increasing the selectivity of the practical catalysts.

Conclusions

It has been shown that by high-throughput FSP method it is possible to prepare large quantities of active and selective Pd catalyst for the acetylene semi-hydrogenation reaction. In particular, the prepared catalyst, reduced *in situ*, achieves a conversion of acetylene of 97% at 500 K and a selectivity to ethylene of 62% at 470 K. Furthermore, these results correlate with the microkinetic simulations based on parameters from extensive DFT calculations over a **$Pd_{30}/Al_2O_3(100)$** model catalyst. The insights gained from this direct comparison can be applied to a parallel computational screening of complex hydrogenation catalysts and synthesis and investigation of the most promising candidates, in the context of both industrial polymerization process and novel applications in the H_2 economy.

Acknowledgements

This work was supported by the European Union's Horizon 2020 research and innovation program through the CritCat Project under Grant Agreement No. 686053. L.P.L.G. is thankful for the support to FCT PhD grant SFRH/BD/128986/2017. This work is also a result of: Project “AIProcMat@N2020 - Advanced Industrial Processes and Materials for a Sustainable Northern Region of Portugal 2020”, with the reference NORTE-01-0145-FEDER-000006, supported by Norte Portugal Regional Operational Programme (NORTE 2020), under the Portugal 2020 Partnership Agreement, through the European Regional Development Fund (ERDF); Associate Laboratory LSRE-LCM – UID/EQU/50020/2019 – funded by national funds through FCT / MCTES (PIDDAC). The DFT calculations were carried out in CSC - the IT Center for Science Ltd., Espoo, Finland.

Appendix A. Supplementary data

Supplementary data to this article can be found online at https://doi.org/10.1016/j.ijhydene.2019.04.086.

REFERENCES

[1] Borodziński A, Bond GC. Selective hydrogenation of ethyne in ethene-rich streams on palladium catalysts. Part 1. Effect of changes to the catalyst during reaction. Catal Rev Sci Eng 2006;48:91–144. https://doi.org/10.1080/01614940500364909.

[2] Spanjers CS, Held JT, Jones MJ, Stanley DD, Sim RS, Janik MJ, et al. Zinc inclusion to heterogeneous nickel catalysts reduces oligomerization during the semi-hydrogenation of acetylene. J Catal 2014;316:164–73. https://doi.org/10.1016/j.jcat.2014.05.007.

[3] Trimm DL, Liu IOY, Cant NW. The selective hydrogenation of acetylene over a Ni/SiO2 catalyst in the presence and absence of carbon monoxide. Appl Catal A Gen 2010;374:58–64. https://doi.org/10.1016/j.apcata.2009.11.030.

[4] Guczi L, Molnár Á, Teschner D. Hydrogenation reactions: concepts and practicevol. 7. Elsevier Ltd.; 2013. https://doi.org/10.1016/B978-0-08-097774-4.00713-0.

[5] Okada Y, Sasaki E, Watanabe E, Hyodo S, Nishijima H. Development of dehydrogenation catalyst for hydrogen generation in organic chemical hydride method. Int J Hydrogen Energy 2006;31:1348–56. https://doi.org/10.1016/j.ijhydene.2005.11.014.

[6] Guo Z, Liu Y, Liu Y, Chu W. Promising SiC support for Pd catalyst in selective hydrogenation of acetylene to ethylene. Appl Surf Sci 2018;442:736–41. https://doi.org/10.1016/j.apsusc.2018.02.145.

[7] Kim SK, Kim C, Lee JH, Kim J, Lee H, Moon SH. Performance of shape-controlled Pd nanoparticles in the selective hydrogenation of acetylene. J Catal 2013;306:146–54. https://doi.org/10.1016/j.jcat.2013.06.018.

[8] Benavidez AD, Burton PD, Nogales JL, Jenkins AR, Ivanov SA, Miller JT, et al. Improved selectivity of carbon-supported palladium catalysts for the hydrogenation of acetylene in excess ethylene. Appl Catal A Gen 2014;482:108–15. https://doi.org/10.1016/j.apcata.2014.05.027.

[9] Molnár Á, Sárkány A, Varga M. Hydrogenation of carbon-carbon multiple bonds: chemo-, regio- and stereo-selectivity. J Mol Catal A Chem 2001;173:185–221. https://doi.org/10.1016/S1381-1169(01)00150-9.

[10] Zhang Q, Li J, Liu X, Zhu Q. Synergetic effect of Pd and Ag dispersed on Al2O3 in the selective hydrogenation of acetylene. Appl Catal A Gen 2000;197:221–8. https://doi.org/10.1016/S0926-860X(99)00463-9.

[11] Osswald J, Giedigkeit R, Jentoft RE, Armbrüster M, Girgsdies F, Kovnir K, et al. Palladium-gallium intermetallic compounds for the selective hydrogenation of acetylene. Part I: preparation and structural investigation under reaction conditions. J Catal 2008;258:210–8. https://doi.org/10.1016/j.jcat.2008.06.013.

[12] Osswald J, Kovnir K, Armbrüster M, Giedigkeit R, Jentoft RE, Wild U, et al. Palladium-gallium intermetallic compounds for the selective hydrogenation of acetylene. Part II: surface characterization and catalytic performance. J Catal 2008;258:219–27. https://doi.org/10.1016/j.jcat.2008.06.014.

[13] Han Y, Peng D, Xu Z, Wan H, Zheng S, Zhu D. TiO2 supported Pd@Ag as highly selective catalysts for hydrogenation of acetylene in excess ethylene. Chem Commun 2013;49:8350. https://doi.org/10.1039/c3cc43511c.

[14] Pei GX, Liu XY, Wang A, Lee AF, Isaacs MA, Li L, et al. Ag alloyed Pd single-atom catalysts for efficient selective hydrogenation of acetylene to ethylene in excess ethylene. ACS Catal 2015;5:3717–25. https://doi.org/10.1021/acscatal.5b00700.

[15] Kim E, Shin EW, Bark CW, Chang I, Yoon WJ, Kim WJ. Pd catalyst promoted by two metal oxides with different reducibilities: properties and performance in the selective hydrogenation of acetylene. Appl Catal A Gen 2014;471:80–3. https://doi.org/10.1016/j.apcata.2013.11.036.

[16] Sárkány A, Weiss AH, Guczi L. Structure sensitivity of acetylene-ethylene hydrogenation over Pd catalysts. J Catal 1986;98:550–3. https://doi.org/10.1016/0021-9517(86)90343-X.

[17] Crespo-Quesada M, Yarulin A, Jin M, Xia Y, Kiwi-Minsker L. Structure sensitivity of alkynol hydrogenation on shape- and size-controlled palladium nanocrystals: which sites are most active and selective? J Am Chem Soc 2011;133:12787–94. https://doi.org/10.1021/ja204557m.

[18] Sheth PA, Neurock M, Smith CM. A first-principles analysis of acetylene hydrogenation over Pd (111). J Phys Chem B 2003:2009–17. https://doi.org/10.1021/jp021342p.

[19] Mei D, Sheth PA, Neurock M, Smith CM. First-principles-based kinetic Monte Carlo simulation of the selective hydrogenation of acetylene over Pd (111). J Catal 2006;242:1–15. https://doi.org/10.1016/j.jcat.2006.05.009.

[20] Ma L, Lv C, Wang G. A DFT study and micro-kinetic analysis of acetylene selective hydrogenation on Pd-doped Cu (111) surfaces. Appl Surf Sci 2017;410:154–65. https://doi.org/10.1016/j.apsusc.2017.01.084.

[21] Yang J, Lv CQ, Guo Y, Wang GC. A DFT+U study of acetylene selective hydrogenation on oxygen defective anatase (101) and rutile (110) TiO2 supported Pd4 cluster. J Chem Phys 2012;136:104107. https://doi.org/10.1063/1.3692292.

[22] Meng LD, Wang GC. A DFT + U study of acetylene selective hydrogenation over anatase supported PdaAgb(a + b = 4) cluster. Phys Chem Chem Phys 2014;16:17541–50. https://doi.org/10.1039/c4cp01818d.

[23] Mädler L, Kammler HK, Mueller R, Pratsinis SE. Controlled synthesis of nanostructured particles by flame spray pyrolysis. J Aerosol Sci 2002;33:369–89. https://doi.org/10.1016/S0021-8502(01)00159-8.

[24] Kovnir K, Armbrüster M, Teschner D, Venkov TV, Szentmiklósi L, Jentoft FC, et al. In situ surface characterization of the intermetallic compound PdGa - a highly selective hydrogenation catalyst. Surf Sci 2009;603:1784–92. https://doi.org/10.1016/j.susc.2008.09.058.

[25] Lock EH, Petrovykh DY, Mack P, Carney T, White RG, Walton SG, et al. Surface composition, chemistry, and structure of polystyrene modified by electron-beam-generated plasma. Langmuir 2010;26:8857–68. https://doi.org/10.1021/la9046337.

[26] Stine R, Petrovykh DY. Oriented self-assembled monolayers of bifunctional molecules on InAs. J Electron Spectrosc Relat Phenom 2009;172:42–6. https://doi.org/10.1016/j.elspec.2009.02.001.

[27] Petrovykh DY, Smith JC, Clark TD, Stine R, Baker LA, Whitman LJ. Self-assembled monolayers of alkanethiols on InAs. Langmuir 2009;25:12185–94. https://doi.org/10.1021/la804314j.

[28] Li Y, Jang BW-L. Selective hydrogenation of acetylene over Pd/Al2O3 catalysts: effect of non-thermal RF plasma preparation methodologies. Top Catal 2017;60:997–1008. https://doi.org/10.1007/s11244-017-0765-5.

[29] CP2K n.d. http://www.cp2k.org (accessed November 3, 2017).

[30] VandeVondele J, Krack M, Mohamed F, Parrinello M, Chassaing T, Hutter J. QUICKSTEP: fast and accurate density functional calculations using a mixed. Gaussian Plane Waves Approach 2005;167:103–28. https://doi.org/10.1016/j.cpc.2004.12.014.

[31] Perdew JP, Burke K, Ernzerhof M. Generalized gradient approximation made simple. Phys Rev Lett 1996;77:3865–8. https://doi.org/10.1103/PhysRevLett.77.3865.

[32] Goedecker S, Teter M, Hutter J. Separable dual-space Gaussian pseudopotentials. Phys Rev B 1996;54:1703–10. https://doi.org/10.1103/PhysRevB.54.1703.

[33] Vandevondele J, Hutter J. Gaussian basis sets for accurate calculations on molecular systems in gas and condensed phases. J Chem Phys 2007;127:114105. https://doi.org/10.1063/1.2770708.

[34] Lippert G, Hutter J, Parrinello M. A hybrid Gaussian and plane wave density functional scheme. Mol Phys 1997;92:477–87. https://doi.org/10.1080/002689797170220.

[35] Grimme S, Antony J, Ehrlich S, Krieg H. A consistent and accurate ab initio parametrization of density functional dispersion correction (DFT-D) for the 94 elements H-Pu. J Chem Phys 2010;132:154104. https://doi.org/10.1063/1.3382344.

[36] Tang W, Sanville E, Henkelman G. A grid-based Bader analysis algorithm without lattice bias. J Phys Condens Matter 2009;21:084204. https://doi.org/10.1088/0953-8984/21/8/084204.

[37] Bader RFW. A quantum theory of molecular structure and its applications. Chem Rev 1991;91:893–928. https://doi.org/10.1021/cr00005a013.

[38] Henkelman G, Uberuaga BP, Jónsson H. A climbing image nudged elastic band method for finding saddle points and minimum energy paths A climbing image nudged elastic band method for finding saddle points and minimum energy paths. J Chem Phys 2016;113:9901–4. https://doi.org/10.1063/1.1329672.

[39] Digne M, Sautet P, Raybaud P, Euzen P, Toulhoat H. Use of DFT to achieve a rational understanding of acid – basic

properties of γ -alumina surfaces. J Catal 2004;226:54–68. https://doi.org/10.1016/j.jcat.2004.04.020.

[40] Honkanen M, Wang J, Kärkkäinen M, Huuhtanen M, Jiang H, Kallinen K, et al. Regeneration of sulfur-poisoned Pd-based catalyst for natural gas oxidation. J Catal 2018;358:253–65. https://doi.org/10.1016/j.jcat.2017.12.021.

[41] Ma L, Melander M, Weckman T, Lipasti S, Laasonen K, Akola J. DFT simulations and microkinetic modelling of 1-pentyne hydrogenation on Cu20 model catalysts. J Mol Graph Model 2016;65:61–70. https://doi.org/10.1016/j.jmgm.2016.02.007.

[42] Ma L, Melander M, Weckman T, Laasonen K, Akola J. CO oxidation on the Au15Cu15 cluster and the role of vacancies in the MgO (100) support. J Phys Chem C 2016;120:26747–58. https://doi.org/10.1021/acs.jpcc.6b06876.

[43] Ma L, Laasonen K, Akola J. Catalytic activity of AuCu clusters on MgO (100): effect of alloy composition for CO oxidation. J Phys Chem C 2017;121:10876–86. https://doi.org/10.1021/acs.jpcc.6b12054.

[44] Brun M, Berthet A, Bertolini JC. XPS, AES and Auger parameter of Pd and PdO. J Electron Spectrosc Relat Phenom 1999;104:55–60. https://doi.org/10.1016/S0368-2048(98)00312-0.

[45] Powell CJ. Recommended Auger parameters for 42 elemental solids. J Electron Spectrosc Relat Phenom 2012;185:1–3. https://doi.org/10.1016/j.elspec.2011.12.001.

[46] Gorzkowski MT, Lewera A. Probing the limits of d - band center theory: electronic and electrocatalytic properties of Pd-shell – Pt-core nanoparticles. J Phys Chem C 2015;119:18389–95. https://doi.org/10.1021/acs.jpcc.5b05302.

[47] Hofmann T, Yu TH, Folse M, Weinhardt L, Ba M, Zhang Y, et al. Using photoelectron spectroscopy and quantum mechanics to determine d - band energies of metals for catalytic applications. J Phys Chem C 2012;116:24016–26. https://doi.org/10.1021/jp303276z.

[48] Molero H, Bartlett BF, Tysoe WT. The hydrogenation of acetylene catalyzed by Palladium : hydrogen pressure dependence. J Catal 1999;181:49–56. https://doi.org/10.1006/jcat.1998.2294.

[49] Babu NS, Lingaiah N, Gopinath R, Sankar Reddy PS, Sai Prasad PS. Characterization and reactivity of alumina-supported Pd catalysts for the room-temperature hydrodechlorination of chlorobenzene. J Phys Chem C 2007;111:6447–53. https://doi.org/10.1021/jp065866r.

[50] Mandal S, Roy D, Chaudhari RV, Sastry M. Pt and Pd nanoparticles immobilized on amine-functionalized zeolite: excellent catalysts for hydrogenation and heck reactions. Chem Mater 2004;16:3714–24. https://doi.org/10.1021/cm0352504.

[51] Strobel R, Krumeich F, Stark WJ, Pratsinis SE, Baiker A. Flame spray synthesis of Pd/Al2O3catalysts and their behavior in enantioselective hydrogenation. J Catal 2004;222:307–14. https://doi.org/10.1016/j.jcat.2003.10.012.

[52] Gigola CE, Aduriz HR, Bodnariuk P. Particle size effect in the hydrogenation of acetylene under industrial conditions. Appl Catal 1986;27:133–44. https://doi.org/10.1016/S0166-9834(00)81052-0.

[53] Teschner D, Borsodi J, Wootsch A, Révay Z, Hävecker M. The roles of subsurface carbon and hydrogen in palladium-catalyzed alkyne hydrogenation. Science 2008;320(80):86–90. https://doi.org/10.1126/science.1155200.